Robust Asymmetric Safety Kalman Filter for MIMO Radar Resisting Temporary Outliers

Eugene Kim, Yoji yamada *Member, IEEE*, and Okamoto shogo *Member, IEEE*

***Abstract*— This study presents a novel concept of robust Kalman filtering especially dealing with outliers when detecting human hand intrusion using multiple-input and multiple-output radar. Outliers that severely deviate from the normal value for a certain period have not been sufficiently discussed from the viewpoint of safety and can seriously hamper the performance of the Kalman filter. Therefore, two types of outliers were intensively discussed, the temporary outlier that originated in miss-detection and the additive outlier that is generated by heavy-tailed error distribution noise. Moreover, an asymmetric outlier processing strategy was proposed depending on positive and negative outliers. The result shows the proposed method can resist the additive and temporary outliers.**

***Index Terms*— Human-robot collaboration, Speed and separation monitoring, Safety-related sensor, 3D human sensing, Unstructured manufacturing**

I. Introduction

Agility and flexibility are crucial in modern production environments [1]. Particularly, classic robot workspace tends to have low productivity owing to being physically separated from the human workers and having low flexibility due to safety fences [2]. Therefore, human–robot collaboration (HRC) plays an important role to meet those modern needs. However, before obtaining the privilege of interacting between the human and the robot, it is necessary to meet the safety guidelines considering potential human–robot contact during HRC [3]. Especially, safety-related protective devices are critical for enabling non-contact-based collaborative modes, including the speed and separation monitoring (SSM) function [4]. In this respect, radar has been considered as a potential candidate for replacing conventional laser scanners as safety-related sensors in HRC, whose performance may degrade under harsh environments where dust, moisture, and smoke coexists [5]–[7]. In fact, radar-based safety-related sensors are already available in the market for HRC safety applications and is expected to be a powerful solution to secure human operators [8].

However, few investigations have been made concerning slow and small object detection issues, such as human hand intrusion, when adopting radio wave-based protective devices [9]. From the viewpoint of productivity and safety, the aforementioned detection issue can be divided based on two aspects: false alarm and miss-detection [10]. In contrast to the false alarm of the radar that has been thoroughly studied, miss-detection of the radar has been barely investigated despite the fact that it can seriously damage the human operator [11], [12]. Especially for the indoor usage of the radar, some studies claimed that there is a chance of encountering a miss-detection, which is the result of ignoring the target by mistake due to the insufficient threshold generating rule against noisy environments [13].

Therefore, in this study, a robust Kalman filtering method is used to reduce the risk of miss-detection. A Kalman filter is the most well-known state-space estimator against observation noise in the field of optimal estimation for target tracking [14]–[17]. However, Kalman filters can be applied only to situations when the profile of the observation noise is a Gaussian distribution, which should be known beforehand [18]. Therefore, applying a robust Kalman filtering method is necessary to improve the quality of the measurement against outliers, which cause large deviations from the normal data [19]. The compensation-based strategy is a solution to this problem. It considers the outlier as an inaccurate measurement and the instant measurement as less reliable observation [20]–[22]. The other approach is the identify-to-reject strategy, which excludes the outlier measurements from the datasets so as to treat the outlier as useless information [23], [24].

Despite many robust Kalman filter schemes that have been proposed to resist the outlier, temporary outliers have not been intensively considered [25]. A possible temporary outlier, such as that generated by miss-detection of the radar, may severely degrade the performance of the radar and cause an instant danger state of the robot [26]. Therefore, this study aims to propose and verify a new approach that can resist the temporary outlier generated by the miss-detection of the radar.

"This work was supported in part by FUJI corporation with their support and technical assistance"

Eugene Kim is with the Department of Mechanical Systems Engineering, Nagoya University, Furo-Cho, Chikusa-ku, Nagoya, 464-8603, Japan

Yoji yamada is with the Department of Mechanical Systems Engineering, Nagoya University, Furo-Cho, Chikusa-ku, Nagoya, 464-8603, Japan

Okamoto shogo is with the Department of Computer Science, Graduate School of Systems Design, Tokyo Metropolitan University, Tokyo 192-0397, Japan

A. Contributions

This study presents a new concept of the Kalman filter approach, enabling the complement of miss-detection and withstanding outliers when detecting human hand intrusion especially using a radio wave sensor. Its core feature is to asymmetrically resist the effect of the outlier according to positive or negative types of error. Another scheme is the identify-to-reject approach for temporary outliers by introducing a temporary judging index based on the Mahalanobis criterion. We showed that the proposed method can mitigate the effect of temporary outliers, which can severely degrade the performance of the conventional identify-to-reject approach.

II. Outlier processing algorithm

In this section, we present the asymmetric extended safety Kalman filter. Note that $\sim$ and $\wedge$ represent measured and estimated values, respectively. In addition, $(+)$ and $(-)$ denote priori and posterior estimations of the state of the space model, respectively. Finally, we classify the outlier as an additive outlier which influences a sole observation, and temporary outlier which causes trends during some temporal time intervals.

A. State space model formulation

We consider the discrete-time nonlinear stochastic state-space model with extended Kalman filter (EKF) [27]. The first process involves the system nonlinear dynamic model, which is expressed as

$$\mathbf{x}_k = f(\mathbf{x}_{k-1}) + \mathbf{w}_k, \tag{1}$$

where $\mathbf{x}_k$ is the n-dimensional state space vector at time k, f is the transition function, and $\mathbf{w}_k$ is a process noise that is assumed to follow the Gaussian distribution.

Next, the state estimate extrapolation process is conducted after performing the measurements as follows:

$$\mathbf{z}_k = h(\mathbf{x}_k) + \mathbf{v}_k, \tag{2}$$

where $\mathbf{z}_k$ is the m-dimensional observation vector at time k, h is the observation function, and $\mathbf{v}_k$ is a measurement noise that is assumed to follow the Gaussian distribution.

Figure 1 shows the overall sequence of the Kalman filter, which is divided into state estimation and error covariance. The first stage of the prediction step is to conduct a prediction of the prior state space that projects the current state $\hat{\mathbf{x}}_k$ and error covariance $\mathbf{P}_k(-)$ forward in time.

$$\hat{\mathbf{x}}_k(-) = f(\mathbf{x}_{k-1}(+)), \tag{3}$$

$$\mathbf{P}_k(-) = \mathbf{F}_k\mathbf{P}_{k-1}\mathbf{F}_k^{\mathrm{T}} + \mathbf{Q}_k, \tag{4}$$

where $\mathbf{x}_{k-1}(+)$ is the estimated space state in discrete time $k-1$ and $\mathbf{Q}$ is the process noise covariance, which satisfies the following:

$$\mathbf{x}_k \sim \mathcal{N}(f(\mathbf{x}_{k-1}), \mathbf{Q}_k). \tag{5}$$

In this study, $\mathbf{F}$ is set as the Jacobian of nonlinear transition function f given by

$$\mathbf{F}_k = \frac{\partial f}{\partial \mathbf{x}}\Big|_{\hat{\mathbf{x}}_{k-1}(+)}. \tag{6}$$

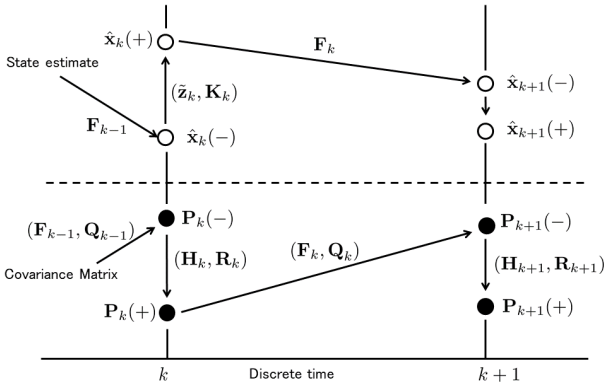

Fig. 1: Representative sequence of values of the Kalman filter variables at discrete-time k. The upper half represents the state estimation process, and the lower half shows the error covariance region

Note that the prediction step of the estimation is based on the constant velocity model.

Next, during the correlation computation stage of the Kalman filtering, Kalman gain $\mathbf{K}$ is calculated using the following formula:

$$\mathbf{K}_k = \mathbf{P}_k(-)\mathbf{H}_k^{\mathrm{T}}[\mathbf{H}_k\mathbf{P}_k(-)\mathbf{H}_k^{\mathrm{T}} + \mathbf{R}_k]^{-1}, \tag{7}$$

where $\mathbf{H}$ is the observation matrix, which is expressed as

$$\mathbf{H}_k = \frac{\partial h}{\partial \mathbf{x}}\Big|_{\hat{\mathbf{x}}_k(-)}, \tag{8}$$

where $\mathbf{R}$ is the measurement noise covariance that satisfies the following:

$$\mathbf{z}_k \sim \mathcal{N}(h(\mathbf{x}_k), \mathbf{R}_k). \tag{9}$$

Finally, state estimation and observational update are carried out in the update stage.

$$\hat{\mathbf{x}}_k(+) = \hat{\mathbf{x}}_k(-) + \mathbf{K}_k[\tilde{\mathbf{z}}_k - h(\hat{\mathbf{x}}_k(-))], \tag{10}$$

where $\mathbf{x}_k(+)$ is the posteri estimation of the state space vector and $\mathbf{K}_k$ is the Kalman gain at discrete time k. In addition, updating the posteriori error covariance $\mathbf{P}_k(+)$ is performed using the following:

$$\mathbf{P}_k(+) = [\mathbf{I} - \mathbf{K}_k\mathbf{H}_k]\mathbf{P}_k(-), \tag{11}$$

where $\mathbf{I}$ is the identical matrix. The equations and algorithms of the extended Kalman filter is briefly explained and summarized in Table I and Algorithm 1.

B. Outlier judgment using Mahalanobis distance

Despite these efforts, in many practical situations, the measurement may not follow the ideal prerequisites, and the erroneous observation that deviates largely from the expected data should be treated differently to that of the normal measurements. Therefore, it needs to identify outliers by the hypothesis test to check if the observation belongs to the assumed model. In this study, the Mahalanobis distance

Algorithm 1: EXTENDED KALMAN FILTER

Input : $\hat{x}_{k-1}(+)$, z_k , P_{k-1}
Output: $\hat{x}_k(+)$, $P_k(+)$

$\hat{x}_k(-) = f(\hat{x}_{k-1}(+))$
$P_k(-) = F_{k-1}P_{k-1}F_{k-1}^{\mathrm{T}} + Q_{k-1}$
$K_k = P_k(-)H_k^{\mathrm{T}}[H_kP_k(-)H_k^{\mathrm{T}} + R_k]^{-1}$
$\hat{x}_k(+) = \hat{x}_k(-) + K_k[z_k - h(\hat{x}_k(-)]$
$P_k(+) = [I - K_kH_k]P_k(-)$
return $\hat{x}_k(+), P_k(+)$

criterion is adopted for the outlier judging index to identify an erroneous outlier [20]:

$$\gamma_k = M_k^2 = (\tilde{\mathbf{z}}_k - h(\hat{\mathbf{x}}_k(-)))^{\mathrm{T}}(\mathbf{P}_k(-))^{-1}(\tilde{\mathbf{z}}_k - h(\hat{\mathbf{x}}_k(-))), \tag{12}$$

where $M_k = \sqrt{(\tilde{\mathbf{z}}_k - h(\hat{\mathbf{x}}_k(-)))^{\mathrm{T}}(\mathbf{P}_k(-))^{-1}(\tilde{\mathbf{z}}_k - h(\hat{\mathbf{x}}_k(-)))}$ is the Mahalanobis distance and γ_k is Gamma judging index that follows the Chi-square distribution with degree of freedom m from the state space vector. An idea of coverage interval was taken into account, which is expressed below, to determine the threshold to judge the outlier using the Mahalanobis distance.

$$C_{\mathrm{p}} \leq 1 - \frac{PFH_{\mathrm{u}}}{DR}, \tag{13}$$

where C_{p} is the coverage probability, DR is the demand rate (demand in hour) of a safety-related system, and PFH_{u} is the upper limit of the probability of failure in an hour [28]. Therefore, the probability threshold α is selected based on the coverage interval criterion:

$$P(\gamma_k \geq \chi_\alpha) = \alpha, \tag{14}$$

where χ_α is the predetermined α-quantile of the Chi-square distribution. With this, several options can be chosen for χ_α with different dangerous failure rate. In this study, based on the required performance level (PL, hereafter) of $PL_{\mathrm{r}} = \mathrm{d}$, it is assumed that α should be higher than $1 - 2.5 \times 10^{-7}$ [29]. Hence, the 2-degree-of-freedom Chi-square distribution with the significance level is $1 - 2.5 \times 10^{-7}$, in which χ_α was set to 30.41.

C. Asymmetric safety extended Kalman filter

Figure 2 shows the concept of a asymmetric safety extended Kalman filter. Based on the observation, outlier judging index $\tilde{\gamma}_\alpha$ is computed for comparison with predetermined χ_α. If $\tilde{\gamma}_\alpha$ is not greater than χ_α, the normal sequence of the Kalman filter is carried out. Conversely, if $\tilde{\gamma}_\alpha$ is greater than the χ_α, and the error isnegative, in other words, where the new measurement is closer than the predicted target point, a compensation process is conducted:

$$\bar{\mathbf{R}}_k = \lambda \mathbf{R}_k, \tag{15}$$

where λ is the scaling factor. As a consequence, (12) should be changed.

$$\bar{\gamma}_k = (\tilde{\mathbf{z}}_k - h(\hat{\mathbf{x}}_k(-)))^{\mathrm{T}}(\bar{\mathbf{P}}_k(-))^{-1}(\tilde{\mathbf{z}}_k - h(\hat{\mathbf{x}}_k(-))), \tag{16}$$

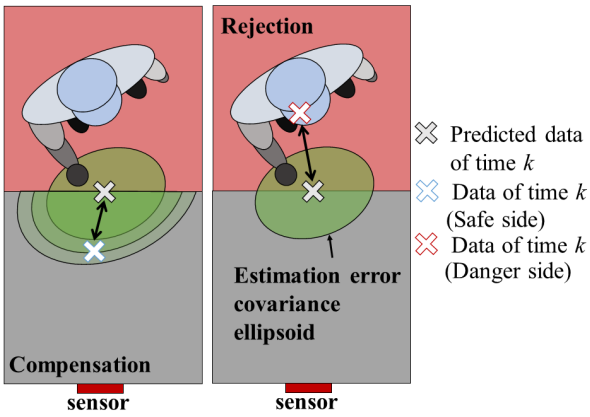

Fig. 2: Concept of the asymmetric Kalman filter using Mahalanobis distance as a outlier judgement. It reacts differently against the positive and negative error. Note that the positive error is a danger side error that may cause the hazardous situation

where

$$\bar{\mathbf{P}}_k(-) = \mathbf{H}_k\mathbf{P}_k(-)\mathbf{H}_k^{\mathrm{T}} + \bar{\mathbf{R}}_k. \tag{17}$$

Next, we used the Newton's method to solve the proper λ_k for non-linearly changing $\bar{\gamma}_k$ [30], letting the function g as

$$g(\lambda_k) = (\tilde{\mathbf{z}}_k - h(\hat{\mathbf{x}}_k(-)))^{\mathrm{T}}(\bar{\mathbf{P}}_k(-))^{-1}(\tilde{\mathbf{z}}_k - h(\hat{\mathbf{x}}_k(-))) - \chi_\alpha = 0. \tag{18}$$

λ_k can be optimized as follows:

$$\lambda_k(i+1) = \lambda_k(i) - \frac{g(\lambda_k(i))}{g'(\lambda_k(i))}, \tag{19}$$

where i is the ith innovation and $'$ is the derivative of the function. Since the derivative of an inverse matrix [31] can be written as:

$$\frac{d}{dt}\mathbf{A}^{-1} = -\mathbf{A}^{-1}\frac{d\mathbf{A}}{dt}\mathbf{A}^{-1}, \tag{20}$$

where $\mathbf{A}$ is a random invertible matrix and function of time t, (19) can be rewritten as

$$\lambda_k(i+1) = \lambda_k(i) + \frac{\bar{\gamma}_k^i - \chi_\alpha}{\mathbf{n}_k^{\mathrm{T}}(\bar{\mathbf{P}}_k^i(-))^{-1}\mathbf{R}_k(\bar{\mathbf{P}}_k^i(-))^{-1}\mathbf{n}_k}, \tag{21}$$

where $\mathbf{n}_k$ represents $(\tilde{\mathbf{z}}_k - h(\hat{\mathbf{x}}_k(-)))$. The initial value of the λ_k should be set to 1 (i.e., $\lambda_k(i) = 1$), and i should be increased until the (16) is equal or less than the predetermined χ_α.

On the contrary, in the case where the error is positive and the measured data is an outlier, the reject strategy is triggered to ignore the measurement noise. In general, updating prior estimation and its covariance is the most used approach in ignoring the measurement [23].

$$\hat{\mathbf{x}}_k(+) = \hat{\mathbf{x}}_k(-), \tag{22}$$

and

$$\mathbf{P}_k(+) = \mathbf{P}_k(-). \tag{23}$$

However, in the case where the temporary outlier is observed, which severely deviates from the normal value for some period

TABLE I: Measurement models and extended Kalman filter equations

System dynamic model:	$\mathbf{x}_k = f(\mathbf{x}_{k-1}) + \mathbf{w}_{k-1}$
Process noise:	$\mathbf{w}_k \sim \mathcal{N}(0, \mathbf{Q}_k)$
Measurement model:	$\mathbf{z}_k = h_k(\mathbf{x}_k) + \mathbf{v}_k$
Measurement noise:	$\mathbf{v}_k \sim \mathcal{N}(0, \mathbf{R}_k)$
State estimate extrapolation:	$\hat{\mathbf{x}}_k(-) = f(\hat{\mathbf{x}}_{k-1}(+))$
Error covariance extrapolation:	$\mathbf{P}_k(-) = \mathbf{F}_{k-1}\mathbf{P}_{k-1}(+)\mathbf{F}_{k-1}^{\mathrm{T}} + \mathbf{Q}_{k-1}$
State estimate observational update:	$\hat{\mathbf{x}}_k(+) = \hat{\mathbf{x}}_k(-) + \mathbf{K}_k[z_k - h(\hat{x}_k(-))]$
Error covariance update:	$\mathbf{P}_k(+) = [\mathbf{I} - \mathbf{K}_k\mathbf{H}_k]\mathbf{P}_k(-)$
Kalman gain matrix	$\mathbf{K}_k = \mathbf{P}_k(-)\mathbf{H}_k^{\mathrm{T}}[\mathbf{H}_k\mathbf{P}_k(-)\mathbf{H}_k^{\mathrm{T}} + \mathbf{R}_k]^{-1}$
State space model $\mathbf{x}$:	$[x, y, V, \theta]^{\mathrm{T}}$

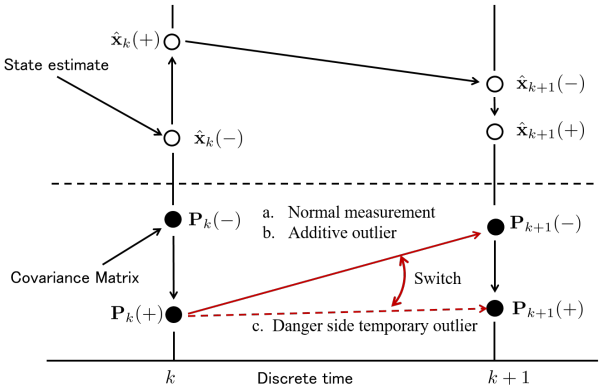

Fig. 3: Representative sequence of values of proposed filter variables at discrete-time k. A temporary outlier judging index τ was adopted to switch to the proposed sequence

can seriously hamper the performance of the Kalman filter. Temporary outlier judging index τ was adopted to count the continuous outliers, as shown in Fig. 3.

$$\mathbf{P}_k(+) = \begin{cases} \mathbf{P}_k(-), & \text{if } \mathbf{n}_k \geq 0, \bar{\gamma}_k^i - \chi_\alpha \geq 0, \tau < 2 \\ \mathbf{P}_{k-1}(+), & \text{if } \mathbf{n}_k \geq 0, \bar{\gamma}_k^i - \chi_\alpha \geq 0, \tau \geq 2, \end{cases} \tag{24}$$

where $\bar{\gamma}_k^i$ is i th iteration of (16). The overall algorithm of the proposed asymmetric safety Kalman filter is summarized in Algorithm 2.

Algorithm 2: ASYMMETRIC SAFETY KALMAN FILTER

Input : $\hat{x}_{k-1}(+)$, z_k , P_{k-1}
Output: $\hat{x}_k(+)$, $P_k(+)$

$\hat{\mathbf{x}}_k(-) = f(\hat{\mathbf{x}}_{k-1}(+))$
$\mathbf{P}_k(-) = \mathbf{F}_{k-1}\mathbf{P}_{k-1}\mathbf{F}^{\mathrm{T}} + \mathbf{Q}_{k-1}$
if $\boldsymbol{n}_k \geq 0$ *and* $\bar{\gamma}_k^i - \chi_\alpha \geq 0$ **then**
  $\hat{\mathbf{x}}_k(+) = \hat{\mathbf{x}}_k(-)$
  if $\tau \leq 2$ **then**
    $\mathbf{P}_k(+) = \mathbf{P}_k(-)$
  else
    $\mathbf{P}_k(+) = \mathbf{P}_{k-1}(+)$
  end
  return $\hat{\mathbf{x}}_k(+), \mathbf{P}_k(+)$
  break
else
  while $\bar{\gamma}_k^i - \chi_\alpha \leq 0$ **do**
    $\bar{\gamma}_k = \mathbf{n}_k^{\mathrm{T}}[\mathbf{H}_k\mathbf{P}_k(-)\mathbf{H}_k^{\mathrm{T}} + \lambda_k\mathbf{R}_k]^{-1}\mathbf{n}_k$
    $\lambda_k^{i+1} = \lambda_k^i + \dfrac{\bar{\gamma}_k^i - \chi_\alpha}{\mathbf{n}_k^{\mathrm{T}}(\bar{\mathbf{P}}_k^i(-))^{-1}\mathbf{R}_k(\bar{\mathbf{P}}_k^i(-))^{-1}\mathbf{n}_k}$
  end
end
$\mathbf{K}_k = \mathbf{P}_k(-)\mathbf{H}_k^{\mathrm{T}}[\mathbf{H}_k\mathbf{P}_k(-)\mathbf{H}_k^{\mathrm{T}} + \lambda_k\mathbf{R}_k]^{-1}$
$\hat{\mathbf{x}}_k(+) = \hat{\mathbf{x}}_k(-) + \mathbf{K}_k[\tilde{\mathbf{z}}_k - h(\hat{\mathbf{x}}_k(-))]$
$\mathbf{P}_k(+) = [\mathbf{I} - \mathbf{K}_k\mathbf{H}_k]\mathbf{P}_k(-)$
return $\hat{\mathbf{x}}_k(+), \mathbf{P}_k(+)$

III. EXPERIMENTAL DESIGN

In this section, the experiment design and general setup are discussed. The experiments aim to investigate the performance of the proposed asymmetric Kalman filter according to the speed of the human hand intrusion. For the comparison between the conventional robust Kalman filters and the proposed one, human hand intrusion test using linear actuator was carried out. As the human hand is small and it is hard for the radar to detect slow objects, it is expected that data of slow motion will contain more outlier generated by miss-detection. Consequently, the proposed filter is expected to resist both the temporary outlier and the typical additive outlier.

A. General setup

Figures 4 and 5 show the hand intrusion test using a test piece (ABS, IEC 61496-3) and the experimental layout of the measurement condition, respectively. In addition, the human mannequin (soft urethane material surfaced) was placed behind

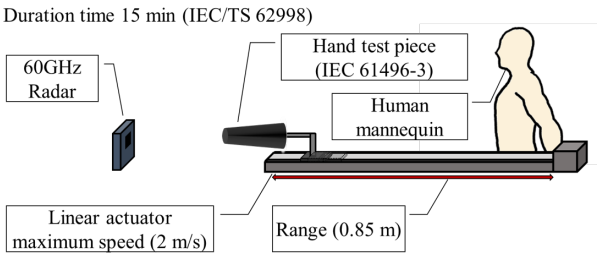

Fig. 4: Experimental design using test piece (IEC 61496-3)

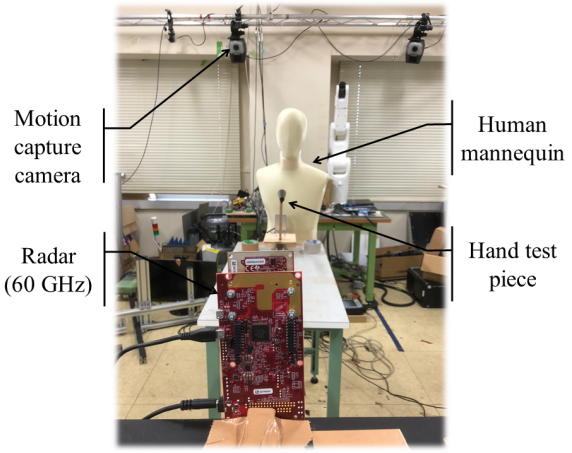

Fig. 5: Experimental layout of the measurement condition. Linear actuator is used for generating back and forth motion of the hand test piece

the linear actuator to represent realistic human hand intrusion conditions. The duration of the experiment was set to 15 min, which is the same as the demand rate in the IEC/TS 62998 [28], and a linear actuator (LEFB25S2S-1000-S2A1, SMC, Japan) was used to move the hand test piece back and forth repeatably (0.85 cm) [32]. To measure the hand test piece, MIMO radar (IWR6843ISK, Texas instruments, America) implemented with 60 GHz standard antenna was used (azimuth and elevation field of view: ±60 and ±20 respectively). The transmit power was 12 dBm with maximum bandwidth of 4 GHz in from 60∼64 GHz. The chirp frequency slope was set to 71.26 MHz/us, and the sampling rate was 5279 ksps, which gives 222 samples for each frequency modulation chirps. In addition, the range resolution using the FFT size of 256 is calculated as 4.34 cm with the measurement rate of 30 Hz.

B. Point cloud processing parameter

The overall measurement system was managed using the Robot Operating System (ROS)-Melodic running on Linux Ubuntu 18.04 LTS (64-bit) [33]. The three-dimensional point clouds are measured by the TI mmwave ros package, which is officially provided by the manufacturer with calibration files and serial drivers needed to execute communication between PC [1]. All the point clouds and closest distance points extracted by the Euclidean clustering method were recorded by the rosbag package with time stamped data. For the comparison, a motion capture system (Motion Analysis Co., Santa Rosa, CA, USA) using twelve cameras was used to measure the relative distance, the velocity between the three-dimensional position of the sensor antenna, and the end tip of the hand test piece. Note that the measured values of the motion capture system are treated as the true values in this experiment.

[1]https://github.com/radar-lab/ti_mmwave_rospkg

C. Performance test under outlier coexistence using Gaussian mixture model

Gaussian mixture model is used to generate two or more complicated noise signal. First, the heavy-tailed Gaussian noise distribution [34] can be generated with following:

$$\mathbf{v}_k \sim (1-\lambda)\mathcal{N}(0, \mathbf{R}_k) + \lambda\mathcal{N}(0, \alpha\mathbf{R}_k), \tag{25}$$

where $\boldsymbol{v}_k$ is the measurement error vector, $\boldsymbol{R}_k$ is the measurement error covariance, λ is the contamination ratio, and α is the scale factor. In detail, λ contributes frequency of outlier generation, and α is related to the magnitude of the outlier when observed.

Second, considering the temporary outlier is observed when the primary target is lost and immediately shifts to the secondary target, the temporary heavy-tailed Gaussian noise is generated as follows:

$$\begin{aligned}\mathbf{z}_k \sim\ & (1-\lambda)\pi_k\mathcal{N}(h(\mathbf{x}_k), \mathbf{R}_k) + \lambda\pi_k\mathcal{N}(h(x_k), \alpha\mathbf{R}_k) \\ & + (1-\pi_k)\mathcal{N}(\mathbf{z}'_{k-1}, \mathbf{R}_k)\end{aligned} \tag{26}$$

where $\boldsymbol{z}_k$ is the observation vector of the primary target, $\boldsymbol{z}'_{k-1}$ is the observation vector of the secondary target, and ρ is the temporary contamination ratio that contributes to the generation of a temporary outlier. In addition, π_k is a Bernoulli variable depending on ρ

$$p(\pi_k|\rho) = \rho^{\pi_k}(1-\rho)^{1-\pi_k}. \tag{27}$$

Finally, it is important that the valid range for generating adequate noise profile by changing parameters are different to each other: $1 < \alpha$, $0 < \lambda < 1$, and $0 < \rho < 1$.

The root means square error (RMSE) is used as an option for the evaluation factor for the performance resisting to the outlier.

$$\text{RMSE} = \frac{1}{N}\sum_{k=1}^{N}\sqrt{\frac{1}{L}\sum_{i=1}^{L}(\mathbf{x}_k^i - \hat{\mathbf{x}}_k^i(+))^2}, \tag{28}$$

where L is the number of trials for the Monte-Carlo simulation and N is the number of the observation vector samples included in each trail.

IV. Results

The fast and slow back-and-forth motion of the test piece was tested to monitor the difference of outlier ratio against the speed of the target object, as shown in Section III-A. Moreover, an analog pulse signal was generated with less than 1 ms of delay to synchronize the measurement time of the motion capture camera and the radar rosbag recording.

Furthermore, the initial conditions of Kalman variables were set as follows: error covariance $\mathbf{P}_0 = \mathbf{Q}_k$; initial space state $\mathbf{x}_0$ with $\hat{\mathbf{x}}_0 = \tilde{\mathbf{z}}_0$; measurement noise covariance as $\mathbf{R}_k = \text{diag}(0.05, 0.05)$; and process noise covariance as $\mathbf{Q}_k = \text{diag}(0.01, 0.01, 0.10, 5)$. For comparison, we considered the conventional EKF applied with the robust method OD-KF (OD-EKF, hereafter) as it has the most powerful outlier resistance performance [23].

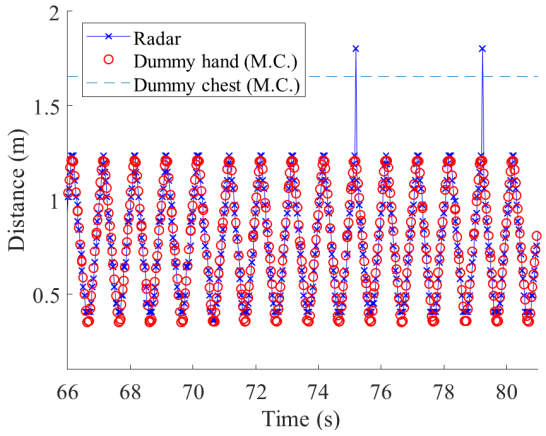

Fig. 6: Typical example of measuring relative distance during the fast-motion trial in some epoch. The additive outlier is dominantly observed compared to the result of the slow motion. The M.C represents the relative distance from the radar and the hand test piece measured by the motion capture system.

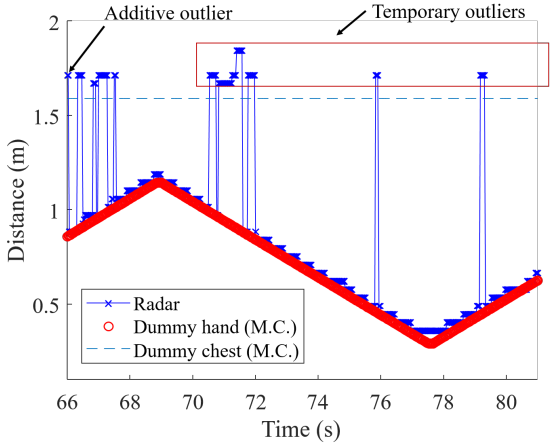

Fig. 7: Typical example of relative distance measurement between the radar and the hand test piece during the slow-motion trial in some epoch. The temporary and additive outliers are observed due to the target shift from hand test piece to a human mannequin body. The M.C represents relative distance from the radar and the hand test piece measured by the motion capture system.

A. Comparison of the outlier ratio depending velocity of the hand test piece

Figure 6 shows the observation data of the relative distance at some epoch during the fast-motion trial. As a result, the ratios of the normal data and the outlier when the speed of the target object is fast motion were 97.5 % and 2.5 %, respectively. In addition, among the entire measurement, the ratios of the additive and temporal outliers when the speed of the target object is slow motion were 1.5 % and 1.0 %, respectively.

Figure 7 shows the typically encountered mixture of temporary and additive outliers during the experiment of slow motion. As a result, the ratios of the normal data and the outlier when the speed of the target object is slow motion were 84.8 % and 15.2 %, respectively. In addition, among the entire measurement, the ratios of the additive and temporal outliers when the speed of the target object is slow motion were 00.2 % and 15.0 %, respectively.

Based on the result, the outlier is six times more often encountered during the slow motion of the target object than the fast motion. Also, among the outliers, the ratio of the temporary outlier increased from 40 % to 99 %.

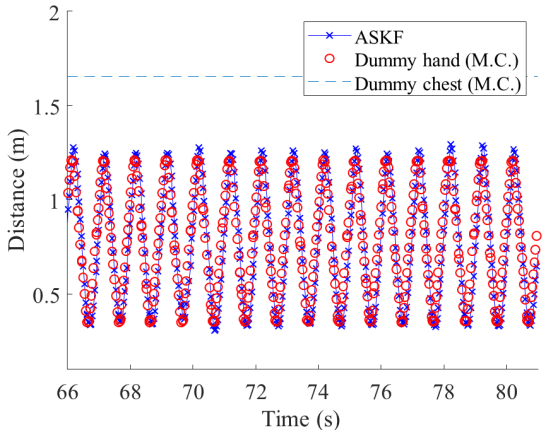

Fig. 8: Result after applying the proposed asymmetric safety Kalman filter during the fast motion of the target object. The result shows the proposed filter can resist to the additive outlier

B. Effect of applying asymmetric safety Kalman filtering methods

Figure 8 shows the data after applying the proposed method during the fast motion of the target object of the relative distance at some epoch. As a result, the ratios of the normal data and the outlier when the speed of the target object is fast motion were 99.6 % and 0.04 %, respectively, which is the decreased value by 84 % compared to that of the raw measurement of the radar. In addition, among the entire measurement, the ratio of additive and temporal outliers when the speed of target object is fast motion were 0.3 % and 0.38 %, respectively, which are decreased by 80 % and 62% compared to that of the raw measurement of the radar, respectively.

Figure 9 shows the data after applying the proposed method during the slow motion of the target object of the relative distance at some epoch. As a result, the ratios of the normal data and the outlier when the speed of the target object is slow motion were 99.4 % and 0.06 %, respectively, which is a decreased value by 99.6 % compared to that of the raw measurement of the radar. In addition, among the entire measurement, the ratios of the additive and temporal outliers when the speed of the target object is slow motion were 1.4×10^{-3} % and 0.06 %, respectively, which is the decreased value by 99.3 % and 96% compared to that of the raw measurement of the radar, respectively. Finally, the overall result of the presented experiment is summarized in Fig 10.

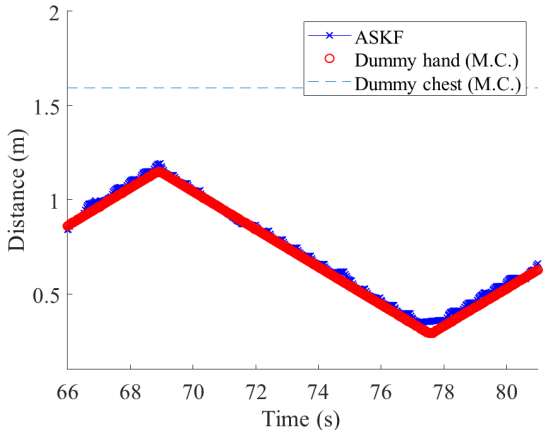

Fig. 9: Result after applying the proposed asymmetric safety Kalman filter during the slow motion of the target object. The result shows the proposed method can resist both the additive and temporary outliers.

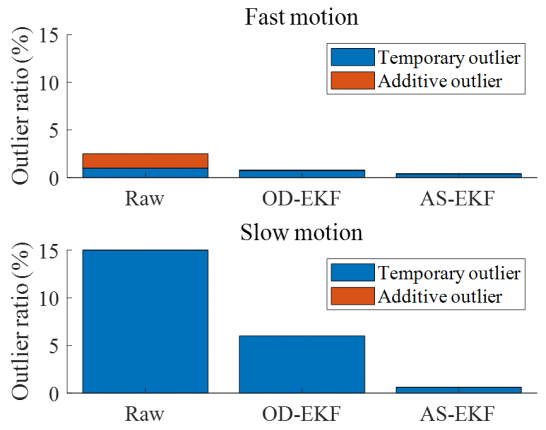

Fig. 10: Summary of the outlier resisting the outlier performance against fast and slow motions of the target object. It is more likely to encounter the temporary outlier when the target is slow. Moreover, the result shows the proposed asymmetric Kalman filter can resist not only to the additive outlier, but also to the temporary outlier

C. Sensitivity analysis using the Monte-Carlo simulation

Figure 11 shows a comparison of the outlier ratio of both temporary and additive outliers for conventional heavy-tailed Gaussian mixture model and the proposed temporary heavy-tailed Gaussian mixture model. Recall that the noise profiles are generated with (26) using $\boldsymbol{z}'$, which is the position data of the secondary target.

Figure 12 shows an example of the generated temporary heavy-tailed Gaussian mixture model noise applied to the position of the hand test piece measured by the motion capture system. From the result, the temporary outlier ratio can be controlled by changing the ρ.

Figure 13 shows a comparison of the generated temporary heavy-tailed Gaussian noise and the proposed asymmetric safety Kalman filter.

TABLE II: Comparison of the danger side outlier proportion when $\alpha = 5$ and $\lambda = 0.15$

ρ	0.05	0.2	0.35	0.50	0.65
AS-KF	1.1×10^{-7}	2.6×10^{-7}	2.6×10^{-7}	2.7×10^{-7}	5.2×10^{-7}
OD-KF	1.4×10^{-7}	4.8×10^{-7}	1.4×10^{-6}	1.5×10^{-5}	1.1×10^{-4}

TABLE III: Comparison of the danger side outlier proportion when $\alpha = 7$ and $\lambda = 0.3$

ρ	0.05	0.2	0.35	0.50	0.65
AS-KF	7.4×10^{-7}	2.3×10^{-6}	3.2×10^{-6}	3.7×10^{-6}	3.4×10^{-6}
OD-KF	2.6×10^{-6}	4.7×10^{-6}	9.2×10^{-6}	2.7×10^{-5}	1.3×10^{-4}

Figure 14 shows the summarized result of comparison between the proposed asymmetric safety Kalman filter and the OD-KF. For a fair comparison between the proposed filter and the OD-KF, 100 rounds for each simulation were given ($L = 100$), and 26,000 observation vector samples generated by the temporary heavy-tailed Gaussian noise were used. As a result, when α and λ increased, RMSE also increased for both the proposed filter and the OD-KF. In addition, there was not much difference between the proposed filter and the OD-KF when ρ was less than 0.2. However, the RMSE increased in the case of using the OD-KF when ρ was larger than 0.5. On the other hand, when using the proposed filter, even the ρ was larger than 0.5, RMSE did not grow higher.

Figure 15 shows the summary of proportion to mistakenly adopt danger side outlier during Monte-Carlo simulation for each cases. Note that the danger side outlier is considered to compare only the miss-detected measurements.

Table II shows the comparison of the danger side outlier proportion when $\alpha = 5$ and $\lambda = 0.15$. The proportion of outliers gets larger for both AS-KF and OD-KF as the temporary contamination ratio ρ gets bigger. However, there is the difference that the outlier proportion is always lower for AS-KF than that of the OD-KF. Table III shows the comparison of the danger side outlier proportion when $\alpha = 7$ and $\lambda = 0.3$. Moreover, with the same result when different cases, the outlier proportion was larger for the case of using OD-KF than that of the AS-KF. This result indicates that the proposed AS-KF can resist temporary outliers.

V. Discussions

A. Relationship of the relative velocity and outlier ratio

As expected, a more temporary outlier was observed in the slow-motion of the test piece rather than the fast motion. This is the result of miss-detection that includes the severity of multi-path and low signal-to-noise ratio (Fig. 10). It is challenging to distinguish the target object from the noisy signals because the signal of the indoor clutter is likely to be stronger than the target signal (wall, ceiling, or background object). In the case where a threshold of the peak signal is set only by considering the false alarm, which is usually determined by the prior knowledge of the measuring condition,

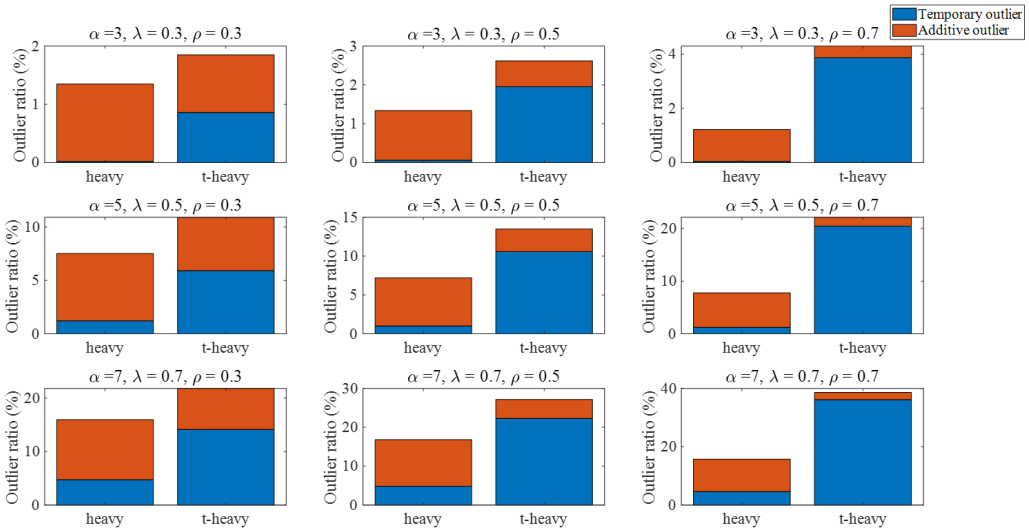

Fig. 11: Summary of generated noise profile used in the Monte-Carlo simulation as shown in (26). The temporary heavy-tailed Gaussian mixture model can generate temporary outlier more than heavy-tailed Gaussian mixture model

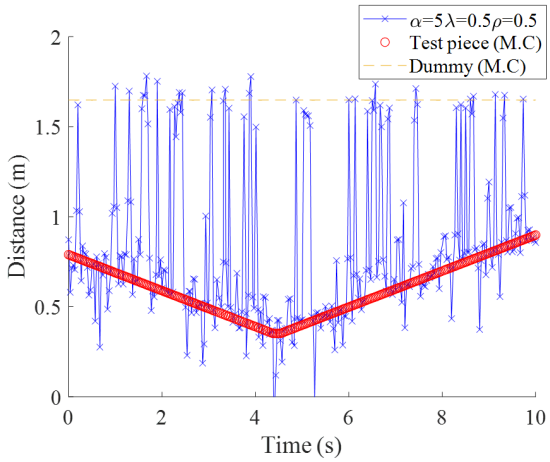

Fig. 12: Example of the generated temporary heavy-tailed Gaussian noise applied to measured position of the hand test piece by the motion capture system ($\alpha = 5$, $\lambda = 0.5$, and $\rho = 0.5$)

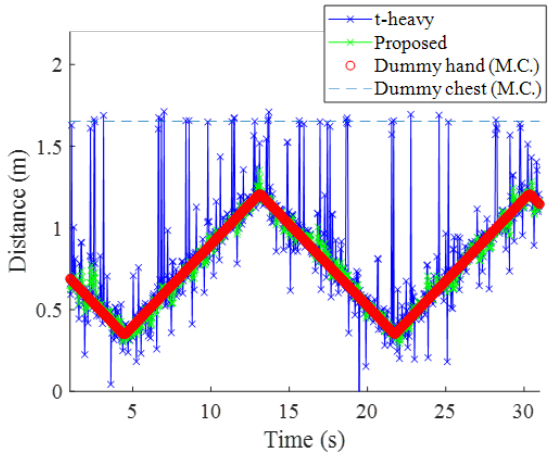

Fig. 13: Comparison of the relative distance calculated by estimating of the proposed asymmetric safety Kalman filter and generating temporary heavy-tailed Gaussian noise ($\alpha = 5$, $\lambda = 0.5$, and $\rho = 0.5$). From the result, the proposed filter can resist both the additive and temporary outliers.

there is a possibility of miss-detection [11], [35], [36]. With this, the presented experiment result shows that the probability of the existence of miss-detection might vary depending on the velocity of the target object.

Despite only a few studies that focus on miss-detection, recent studies in the IR-UWB field now emphasize the critical problem of the target loss and miss-detection. In this regard, Quan et al. proposed a constant miss detection rate (CMDR), which can complement the conventional constant false alarm rate [26]. However, as the authors suggest, the ratio of outlier varies against hyper-parameters and can be easily changed, and the result of the probability of detection failure is not sufficient to meet the safety criteria. Therefore, in parallel to the approach of the dynamic thresholding method, the stochastic approach presented in this study can be applied to complement the insufficient ability to resist the outlier. However, the result of the presented experiment only holds with a specific frequency of used radio wave, and the type of frequency modulation should be considered because the reflectively and the radar-cross section level may vary against measurement conditions [37].

B. Temporary outlier and rejection strategy

The experiment results show that a Kalman filter that only uses the identify-to-reject strategy might ignore the chance of human intrusion, as shown in (Fig. 15. The proposed asymmetric safety Kalman filter can resist both the additive and temporary outliers. This is because the design of the proposed filter adapts an identify-to-reject strategy only against the

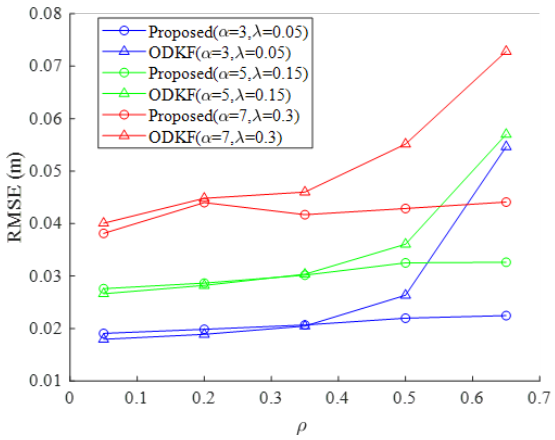

Fig. 14: Result of comparing root means square error between the proposed asymmetric safety Kalman filter and the ODKF. Each color represents results for the same condition for generating temporary heavy-tailed Gaussian noise. Note that RMSE is computed with Monte-Carlo simulation ($L = 100$,$N = 26,000$)

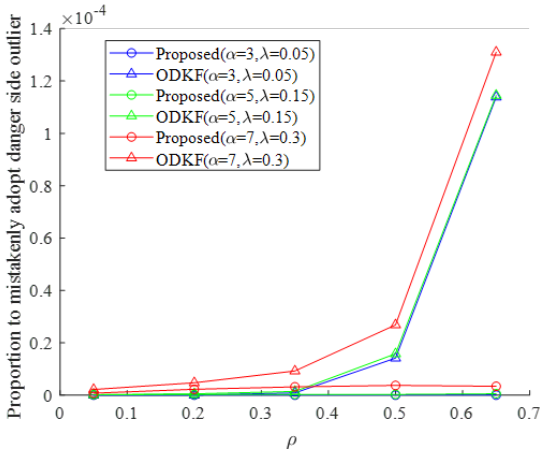

Fig. 15: Comparison of the danger side outlier proportion to adopt the outlier during the Monte-Carlo simulation

dangerous side outlier to resist temporary outliers. Therefore, the issue that mistakenly considers the human body intrusion as an outlier can be solved using the filter with the asymmetric strategy suggested in this study.

Meanwhile, there are several items to consider due to the inherent problem of the proposed method, especially the Kalman filter. In practical measurement situations, it is very difficult to determine the process noise accurately and to say that the noise profile for the unknown object employed in the related research is applied to all situations. Moreover, the outlier judging index that follows the gamma variance may need to be set less strictly in some cases. Therefore, the parameters presented in this study need to be precisely tuned according to the main target or the measurement environment not to judge them as outliers or temporary outliers too easily. As a follow-up study, if simulation methods suggested in this study are used, the sensitivity of each of the Kalman parameters may possibly be evaluated.

C. Contamination parameters for the reproduction of an actual human intrusion measurement profile

In this study, an intensive Monte-Carlo simulation was conducted based on the temporary heavy-tailed Gaussian distribution, which reproduces the known measurement error, additive outlier, and temporary outlier (Fig. 15). One of the problems of generating outliers using conventional heavy-tailed Gaussian distribution was that the ratio of the temporary and additive outliers was fixed following the relative velocity between the target and the radar (Fig. 10). However, the proposed temporary heavy-tailed Gaussian noise model can adjust the ratio of additive and temporary outliers. Therefore, the proposed noise model can aid temporary outlier-related studies, and further discussions are needed to supplement the noise parameters, such as the temporary contamination ratio, to generate more realistic noise conditions.

Meanwhile, the experiment result of the intrusion of the test piece suggests that the outlier ratio can differ against the relative velocity between the radar and the target (Fig. 10). The relative velocity can be an element consisting of the noise parameters, such as the contamination ratio λ and temporary contamination ratio ρ, even though the result needs additional validation using an actual human body intrusion (26). Therefore, the validation process should meet the required prerequisites including various intrusion patterns and scenarios to reproduce realistic measurement noise conditions.

D. Applications to different measurement conditions

Each simulation case is considered to account for the ability of the proposed filter in resisting more extreme conditions (Table II, III) The result for each case using different temporary outlier ratios ρ shows that the proposed filter can be applied to more extreme conditions, which include dynamic measurement environments. However, when α and λ are relatively high, the proposed filter has a limitation in terms of RMSE increasing. Therefore, when using the protective equipment in extreme conditions that may largely degrade the measurement performance, it seems natural to increase redundancy by integrating additional safety-related sensors to meet the required safety integrity level. Furthermore, one of the main challenges when applying the proposed filtering technique is obtaining noise profiles with extensive testing in actual usage conditions. Therefore, relevant parameters should be carefully tuned in a manner that reduces the outlier the most and mistakenly chosen parameters may lead to overestimating or underestimating those outliers.

Conversely, additional concerns arise in the case where multiple targets interact within the shared workspace of humans and robots. Note that the miss-detection rate may increase due to the occlusions originating in the relative placement of the protective equipment and the human. Therefore, the proposed method should be further investigated with additional situations and case studies where multiple trackers are implemented such as the nearest neighbor approach [38].

VI. Conclusion

We proposed the asymmetric safety Kalman filter, which deals with temporary outliers, to detect human body intrusion using multiple-input and multiple-output radar. The temporary outlier, which severely deviates from the normal value for some period, has not been discussed in detail in terms of safety and can seriously hamper the performance of the Kalman filter even with robust techniques. In this study, a human hand intrusion experiment using a hand test piece and intensive Monte-Carlo simulation were carried out. The result shows that the proposed asymmetric safety Kalman filter can resist both the additive and temporary outliers. Therefore, the proposed method can be applied to prevent mistakenly considering human body intrusion as an outlier based on the stochastically outlier judging criterion.

References

[1] S. Robla-Gómez, V. M. Becerra, J. R. Llata, E. Gonzalez-Sarabia, C. Torre-Ferrero, and J. Perez-Oria, "Working together: A review on safe human-robot collaboration in industrial environments," *IEEE Access*, vol. 5, pp. 26 754–26 773, 2017.

[2] J. A. Marvel and R. Norcross, "Implementing speed and separation monitoring in collaborative robot workcells," *Robotics and computer-integrated manufacturing*, vol. 44, pp. 144–155, 2017.

[3] Safety of machinery – General principles for design – Risk assessment and risk reduction, ISO 12100:2010.

[4] Robots and robotic devices–Collaborative robots, ISO/TS 15066: 2015.

[5] M. Zlatanski, P. Sommer, F. Zurfluh, and G. L. Madonna, "Radar sensor for fenceless machine guarding and collaborative robotics," in *2018 IEEE International Conference on Intelligence and Safety for Robotics (ISR)*. IEEE, 2018, pp. 19–25.

[6] E. Kim, Y. Yamada, and S. Okamoto, "Improvement of safety integrity level by multiplexing radio wave sensors," in *System Integration , 2017 IEEE/SICE International Symposium on*. IEEE, 2017, pp. 942–947.

[7] B. K. Kim and Y. Sumi, "Vision-based safety-related sensors in low visibility by fog," *Sensors (Switzerland)*, vol. 20, no. 10, 2020.

[8] Inspect, *LBK system*, 2020 (accessed October 5, 2020), https://www.inxpect.com/en/products/lbk-system/.

[9] E. Kim, Y. Yamada, S. Okamoto, M. Sennin, and H. Kito, "Considerations of potential runaway motion and physical interaction for speed and separation monitoring," *Robotics and Computer-Integrated Manufacturing*, vol. 67, p. 102034.

[10] N. Neogi, "Using intent information to investigate the relationship between missed detections and false alarms in conflict detection verification," in *Digital Avionics Systems Conference, 2003. DASC'03. The 22nd*, vol. 1. IEEE, 2003, pp. 3–B.

[11] M. Barkat, S. Himonas, and P. Varshney, "Cfar detection for multiple target situations," in *IEE Proceedings F (Radar and Signal Processing)*, vol. 136, no. 5. IET, 1989, pp. 193–209.

[12] H. Wu, E. Kim, Y. Yamada, and S. Okamoto, "Cumulative clustering filter for mimo radar detecting human hand intrusion," in *International Conference on Intelligence and Safety for Robotics*. IEEE, 2021, pp. 338–341.

[13] X. Quan, J. W. Choi, and S. H. Cho, "A new thresholding method for ir-uwb radar-based detection applications," *Sensors*, vol. 20, no. 8, p. 2314, 2020.

[14] Z. Yan, T. Duckett, and N. Bellotto, "Online learning for 3d lidar-based human detection: experimental analysis of point cloud clustering and classification methods," *Autonomous Robots*, vol. 44, no. 2, pp. 147–164, 2020.

[15] N. Bellotto and H. Hu, "Computationally efficient solutions for tracking people with a mobile robot: an experimental evaluation of bayesian filters," *Autonomous Robots*, vol. 28, no. 4, pp. 425–438, 2010.

[16] ——, "Multisensor-based human detection and tracking for mobile service robots," *IEEE Transactions on Systems, Man, and Cybernetics, Part B (Cybernetics)*, vol. 39, no. 1, pp. 167–181, 2008.

[17] R. Bodor, B. Jackson, and N. Papanikolopoulos, "Vision-based human tracking and activity recognition," in *Proc. of the 11th Mediterranean Conf. on Control and Automation*, vol. 1, 2003.

[18] G. Agamennoni, J. I. Nieto, and E. M. Nebot, "Approximate inference in state-space models with heavy-tailed noise," *IEEE Transactions on Signal Processing*, vol. 60, no. 10, pp. 5024–5037, 2012.

[19] M. A. Gandhi and L. Mili, "Robust kalman filter based on a generalized maximum-likelihood-type estimator," *IEEE Transactions on Signal Processing*, vol. 58, no. 5, pp. 2509–2520, 2009.

[20] G. Chang, "Robust kalman filtering based on mahalanobis distance as outlier judging criterion," *Journal of Geodesy*, vol. 88, no. 4, pp. 391–401, 2014.

[21] L. Chang and K. Li, "Unified form for the robust gaussian information filtering based on m-estimate," *IEEE Signal Processing Letters*, vol. 24, no. 4, pp. 412–416, 2017.

[22] H. Wang, H. Li, W. Zhang, and H. Wang, "Laplace l1 robust kalman filter based on majorization minimization," in *2017 20th International Conference on Information Fusion (Fusion)*. IEEE, 2017, pp. 1–5.

[23] H. Wang, H. Li, J. Fang, and H. Wang, "Robust gaussian kalman filter with outlier detection," *IEEE Signal Processing Letters*, vol. 25, no. 8, pp. 1236–1240, 2018.

[24] Q. Wan, H. Duan, J. Fang, H. Li, and Z. Xing, "Robust bayesian compressed sensing with outliers," *Signal Processing*, vol. 140, pp. 104–109, 2017.

[25] A. Huang, K. Lai, Y. Li, and S. Wang, "Forecasting container throughput of Qingdao port with a hybrid model," *Journal of Systems Science and Complexity*, vol. 28, no. 1, pp. 105–121, 2014.

[26] X. Quan, J. W. Choi, and S. H. Cho, "A New Thresholding Method for IR-UWB Radar-Based Detection Applications," *Sensors (Switzerland)*, vol. 20, no. 8, pp. 1–24, 2020.

[27] G. Welch, G. Bishop *et al.*, "An introduction to the kalman filter," 1995.

[28] Safety of machinery - Electro-sensitive protective equipment - Safety-related sensors used for protection of person, IEC/TS 62998.

[29] Safety of machinery – Safety-related parts of control systems – Part 1: General principles for design, ISO 13849-1:2015.

[30] J. E. Dennis Jr and R. B. Schnabel, *Numerical methods for unconstrained optimization and nonlinear equations*. SIAM, 1996.

[31] D. Simon, *Optimal state estimation: Kalman, H infinity, and nonlinear approaches*. John Wiley & Sons, 2006.

[32] Safety of machinery – Positioning of safeguards with respect to the approach speeds of parts of the human body, ISO 13855:2010.

[33] M. Quigley, K. Conley, B. Gerkey, J. Faust, T. Foote, J. Leibs, R. Wheeler, and A. Y. Ng, "Ros: an open-source robot operating system," in *ICRA workshop on open source software*, vol. 3, no. 3.2. Kobe, Japan, 2009, p. 5.

[34] Y. Huang, Y. Zhang, N. Li, and J. Chambers, "Robust student'st based nonlinear filter and smoother," *IEEE Transactions on Aerospace and Electronic Systems*, vol. 52, no. 5, pp. 2586–2596, 2016.

[35] H. Rohling, "Radar cfar thresholding in clutter and multiple target situations," *IEEE transactions on aerospace and electronic systems*, no. 4, pp. 608–621, 1983.

[36] P. P. Gandhi and S. A. Kassam, "Analysis of cfar processors in nonhomogeneous background," *IEEE Transactions on Aerospace and Electronic systems*, vol. 24, no. 4, pp. 427–445, 1988.

[37] P. Hügler, M. Geiger, and C. Waldschmidt, "Rcs measurements of a human hand for radar-based gesture recognition at e-band," in *2016 German Microwave Conference (GeMiC)*. IEEE, 2016, pp. 259–262.

[38] A. Sinha, Z. Ding, T. Kirubarajan, and M. Farooq, "Track quality based multitarget tracking approach for global nearest-neighbor association," *IEEE Transactions on Aerospace and Electronic Systems*, vol. 48, no. 2, pp. 1179–1191, 2012.

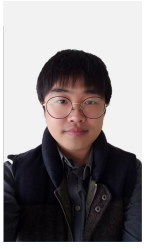

Eugene Kim was born in Busan, Korea, in 1992. He received the B.S. degree in engineering from Nagoya institute of college, Nagoya, Japan, in 2016, and the M.S. degree in engineering from Nagoya University, Nagoya, Japan, in 2018, and the Ph.D. degree in engineering from Nagoya University, Nagoya.

Yoji Yamada (Member, IEEE) received the Ph.D. degree from the Tokyo Institute of Technology. Since 1983, he has been with the Toyota Technological Institute, Nagoya, Japan. In 2004, he joined the Safety Intelligence Research Group, National Institute of Advanced Industrial Science and Technology (AIST), as a Leader. In 2009, he joined the Department of Mechanical Science and Engineering, Graduate School of Engineering, Nagoya University, as a Professor.

Shogo Okamoto (Member, IEEE) received the Ph.D. degree in information sciences from Tohoku University, in 2010. From 2010 to 2021, he was with Nagoya University. He is currently an Associate Professor with the Department of Computer Science, Tokyo Metropolitan University. His research interests include haptics, assistive robotics, human-centered informatics, and affective engineering.